Available online at www.sciencedirect.com
ScienceDirect
Journal of the European Ceramic Society 30 (2010) 605–611
www.elsevier.com/locate/jeurceramsoc

Synthesis and oxygen transport properties of $La_{0.2}Sr_{0.8}Fe_{1-x}Ti_xO_{3-\delta}$ ($x = 0.2$, 0.4) intended for syn-gas production

Eva Bartonickova [a,*], Kjell Wiik [b], Karel Maca [a], Hilde L. Lein [b], Espen A. Rudberg [b]

[a] *Department of Ceramics and Polymers, Brno University of Technology, Technicka 2896/2, Brno, Czech Republic*
[b] *Department of Materials Science and Engineering, Norwegian University of Science and Technology, Trondheim, Norway*

Available online 3 August 2009

Abstract

Perovskites in the system $La_{0.2}Sr_{0.8}Fe_{1-x}Ti_xO_{3-\delta}$ exhibit high stability at severe reducing conditions and high temperatures. Here we report the processing and oxygen transport properties of two compositions: $La_{0.2}Sr_{0.8}Fe_{1-x}Ti_xO_{3-\delta}$ ($x = 0.2$, 0.4). Single-phase powders were synthesized by spray pyrolysis (SP) and solid state reaction (SSR). The resulting average particle sizes (BET) ranged from 140 nm (SP) to 1090 nm (SSR). Samples were prepared by CIP and pressureless sintered between 1200 and 1250 °C for 8–12 h. Sintered densities ranged from 97 (SSR) to 99% (SP) and grain size was less than 1.5 μm. The average TEC varied in the range (13.8–14.6) × 10^{-6} K^{-1} at 300–600 °C and (21.3–28.9) × 10^{-6} K^{-1} at 600–800 °C. Surface exchange coefficients (k_{chem}) and bulk diffusion coefficients (D_{chem}) in terms of temperature and p_{O_2} were assessed by the method of electrical conductivity relaxation. A simple defect model was applied to explain electrical conductivity and bulk diffusion behaviour.

Keywords: A. Powders-solid state reaction; A. Spray pyrolysis; C. Electrical properties; C. Thermal expansion; D. Perovskites

1. Introduction

The development of cost-effective dense ceramic membrane-based reactors for production of syn-gas (H_2–CO) from natural gas is of considerable interest. This technology leans itself to the development of oxides with sufficient mixed conductivity (ionic and electronic) and sufficient stability at severe reducing conditions even at high temperatures. These oxides may be synthesized in a number of different ways, e.g., wet chemical preparation such as sol–gel processes, glycine nitrite combustion reaction[1–3] and spray pyrolysis method.[4–9] Solid state reaction is another well-established way of producing ceramics.[10–13] Electrical conductivity and oxygen transport properties have been studied for a number of highly stable perovskites, such as, e.g., $La_{1-x}Sr_xFe_{1-y}Ti_yO_{3-\delta}$ ceramics.[4,5,14–18] Tsipis et al.[17] measured the total conductivity in air by 4-probe DC and 4-electrode AC method connected to a frequency response analyzer.

The total conductivity was oxygen-ionic and n-type electronic in the oxygen partial pressure range (p_{O_2}) 10^{-14} to 10^{-10} atm. Substitution of Fe and La by Sr and Ti decreased oxygen permeability and partial ionic and electronic conductivities, but also suppressed unfavourable thermal expansion. The thermal expansion behaviour was studied by dilatometry showing the tendency of a decreasing thermal expansion coefficient (TEC) with increasing Ti-substitution on B-site. Kaus et al.[5] and Yoo et al.[11] performed conductivity relaxation measurements by a four-point method technique in flow of air and CO/CO_2 mixtures. The total conductivity was measured at 727 °C and oxygen partial pressure 10^{-16} atm. They reported oxygen ionic conductivities based on electrical conductivity- and oxygen flux measurements. The highest electrical conductivities were obtained in samples with the highest Fe-content ($La_{0.5}Sr_{0.5}Fe_{0.8}Ti_{0.2}O_{3-\delta}$) corresponding to 52 S/cm. Chemical expansion and oxygen flux could be explained by a simple defect model. Park et al.[4,18] measured the electrical conductivity by AC and DC four-point method at temperatures between 20 and 900 °C and p_{O_2} between 5 × 10^{-5} atm and 1 atm. TG-analysis showed that oxygen loss was initiated at approx. 220 °C coinciding with a decrease in conductivity. Fagg et al.[14–16] performed the total conductivity measurement by four-point electrode AC method using a frequency response analyzer. The experiments were performed at controlled humidity and atmosphere. They reported data showing the decreasing tendency of ionic and p-type conductivities with La addition as well as with increasing the A-site deficiency, while the effect of increasing Fe cation

* Corresponding author. Tel.: +420 541143340; fax: +420 541143202.
E-mail address: bartonickova@fme.vutbr.cz (E. Bartonickova).

0955-2219/$ – see front matter © 2009 Elsevier Ltd. All rights reserved.
doi:10.1016/j.jeurceramsoc.2009.06.037

concentration was opposite. At reducing conditions the n-type conductivity was studied and found to increase with A-site La-substitution. The influence of substitution of La with Sr on thermal expansion behaviour was studied and the reported data showed the increase of TEC values with increasing Sr-doping.

The goal of our work was to prepare high density bulk materials with two different compositions ($La_{0.2}Sr_{0.8}Fe_{1-x}Ti_xO_{3-\delta}$, where $x = 0.2$ and 0.4), based on ceramic powders synthesized by two different methods, namely solid state reaction and spray pyrolysis, respectively. The thermal and chemical expansion behaviour and oxygen transport properties of both compositions are also investigated both in terms of temperature and oxygen partial pressure.

2. Experimental procedure

2.1. Powder synthesis

Perovskites in the system $La_{0.2}Sr_{0.8}Fe_{1-x}Ti_xO_{3-\delta}$ ($x = 0.2$, 0.4; designated in the further text as LSFT20 and LSFT40, resp.) were synthesized by two methods, namely solid state reaction (SSR) and spray pyrolysis (SP), respectively. The carbonates and oxides were used as starting materials for the SSR method. The suspensions of stoichiometric ratios of starting materials in isopropanol were planetary ball-milled (zirconia balls/0.5 cm) for 12 h and then the high temperature solid state reaction in air at 1100 °C for 30 h was performed. Products of these syntheses are marked as LSFT20_SSR and LSFT40_SSR in the following text. Spray pyrolysis was performed from stoichiometric aqueous solutions of nitrates and alkoxides of each cation. Details of spray pyrolysis procedure are given elsewhere.[4–9] The as-synthesized precursors were calcined at 900 °C for 2 h then ball milled in ethanol for 12 h and dried. Products of these syntheses are marked as LSFT20_SP and LSFT40_SP.

2.2. Ceramic shaping and sintering

The bar-shaped green bodies of LSFT20 were prepared by unaxial pressing (2 kN) followed by cold isostatic pressing (CIP – 200 MPa). The prepared bodies were sintered in air at 1200 °C for 8–12 h and slowly cooled in order to achieve equilibrium with air on cooling. The sintered bars were cut, grinded and polished to final dimensions of approximately 4.0 mm × 5.0 mm × 21.0 mm. The pellet-shaped green bodies of LSFT40 were prepared by cold isostatic pressing (CIP – 300 MPa) and grinded to dimensions of approximately 5.0 mm × 5.0 mm × 25.0 mm before sintering. Those as-prepared bodies were sintered at 1250 °C for 10 h and slowly cooled in order to achieve equilibrium with air on cooling and polished to final dimensions approximately 4.0 mm × 4.0 mm × 21.0 mm.

2.3. Ceramic characterization

The phase composition was determined by X-ray diffraction analysis, K_{Co} wavelength (X'pert, Philips, Netherlands). The morphology of powder products was studied by scanning electron microscopy (SEM XL 30, Philips, Netherlands and Hitachi s-3500, Japan). The specific surface area (SSA_{BET}) was determined by the BET method (Chembet Quantachrome, USA) and size of agglomerates was measured by means of laser diffraction analysis (Horiba LA 950, Japan). The final density of ceramic bodies was measured by means of Archimedes method with distilled water as liquid media. Theoretical (crystallographic) density of individual materials was calculated with the help of lattice parameters determined by Rietveld analysis. The pore size distribution was measured by mercury porosimetry (Pascal 440 Porotec, Germany). The thermal expansion behaviour was studied by dilatometry on sintered bodies in air at a heating rate of 2 K/min (NETZCH DIL 402C, Germany). Coefficient of thermal expansion (TEC) was calculated from dilatometric curves of sintered samples.[19] The electrical conductivity relaxation technique was used to assess the total conductivity and the oxygen transport properties (D_{chem} and k_{chem}).[5,11] The electrical behaviour and transport properties were studied at temperatures between 800 and 1050 °C and oxygen partial pressures ranging from 0.2 to 0.02 atm in O_2/N_2 mixtures. The total conductivity was measured by a four-point method by monitoring the voltage drop across a well-defined sample dimension.

3. Results and discussion

3.1. Powders characterization

XRD analysis showed that single-phase powders of $La_{0.2}Sr_{0.8}Fe_{0.8}Ti_{0.2}O_{3-\delta}$ (LSFT20) and $La_{0.2}Sr_{0.8}Fe_{0.6}Ti_{0.4}O_{3-\delta}$ (LSFT40) were prepared by both synthesis methods – solid state reaction and spray pyrolysis and (see Fig. 1). The lattice symmetry is cubic and space group is *Pm*3*m*.

Table 1 compares the particle size of calcined and milled powders determined by BET and by laser diffraction. The corresponding microstructure is given in Fig. 2(a)–(d). It can be seen that particle size calculated from BET corresponds quite well

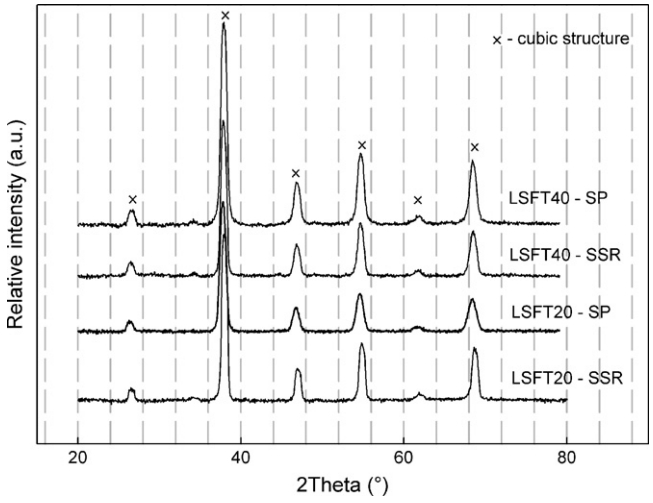

Fig. 1. XRD patterns of prepared ceramics powders via two methods in two compositions (LSFT20, 40_SP – calcined at 900 °C for 2 h; LSFT20, 40_SSR – calcined at 1100 °C for 30 h).

Table 1
Specific surface areas and particle size of prepared powders.

Sample	BET (m^2/g)	Particle size calc. from BET (μm)	Particle size LD (μm)
LSFT20_SP	4.12	0.22	1.32
LSFT40_SP	7.78	0.14	4.40
LSFT20_SSR	1.00	1.09	1.45
LSFT40_SSR	3.04	0.36	1.31

with size of primary particles while values measured by laser diffraction with agglomerate sizes. Particle sizes were in the range of 140–360 nm, only LSFT20_SSR powder had particle size slightly higher than 1 μm.

Raw powders prepared by spray pyrolysis were typically hollow spherically shaped agglomerates (Fig. 2(c) and (d)) with a primary particle size between 140 and 220 nm (Table 1). The large particle size observed by laser diffraction (Table 1) probably reflects the average agglomerate size.

3.2. Shaping and sintering of ceramic bodies

Green bodies were made from the powders by cold isostatic pressing. Fig. 3 shows the pore size distribution in LSFT40 green bodies as measured by mercury porosimetry. It can be seen that pores in green bodies were several times smaller than primary particles (2 times for LSFT40_SSR, 2.5 times for LSFT40_SP, and even 3.5 times for milled LSFT40_SP) which is an indicator of good sintering behaviour.[20] The small size of pores indicates that agglomerates are soft and were destroyed during pressing.

As can be seen from Table 2 we were able to sinter all samples to a final density higher than 96.7% of the theoretical density,

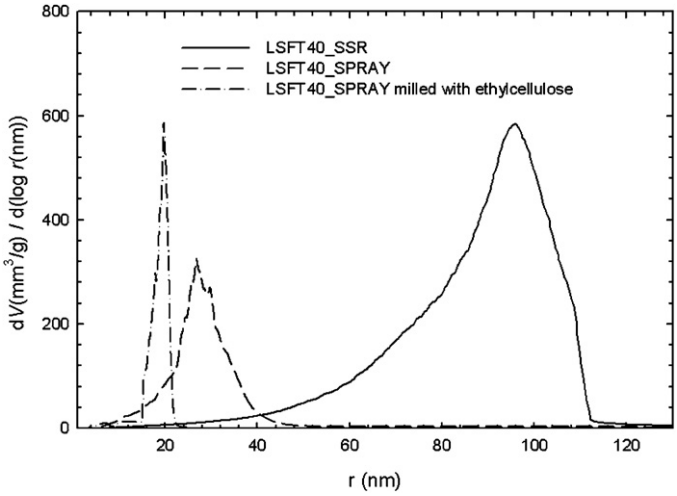

Fig. 3. Pore size distribution measured by mercury porosimetry.

Table 2
Sintering conditions, theoretical densities and final densities of sintered bodies.

Sample	Sintering (°C/h)	ρ_{theor} (g cm^{-3})	ρ (g cm^{-3})	ρ_{rel} (% t.d.)
LSFT20_SP	1200/10	5.51	5.43	98.52
LSFT40_SP	1200/10	5.58	5.52	98.82
LSFT20_SSR	1200/10	5.52	5.34	96.73
LSFT40_SSR	1250/10	5.58	5.42	97.87

corresponding to closed porosity stage and thus qualifying all samples for characterization of oxygen transport properties.

Both compositions based on spray pyrolysed powders obtain densities close to 99%. This high density is basically due to the small primary particle size resulting from spray pyrolysis (140

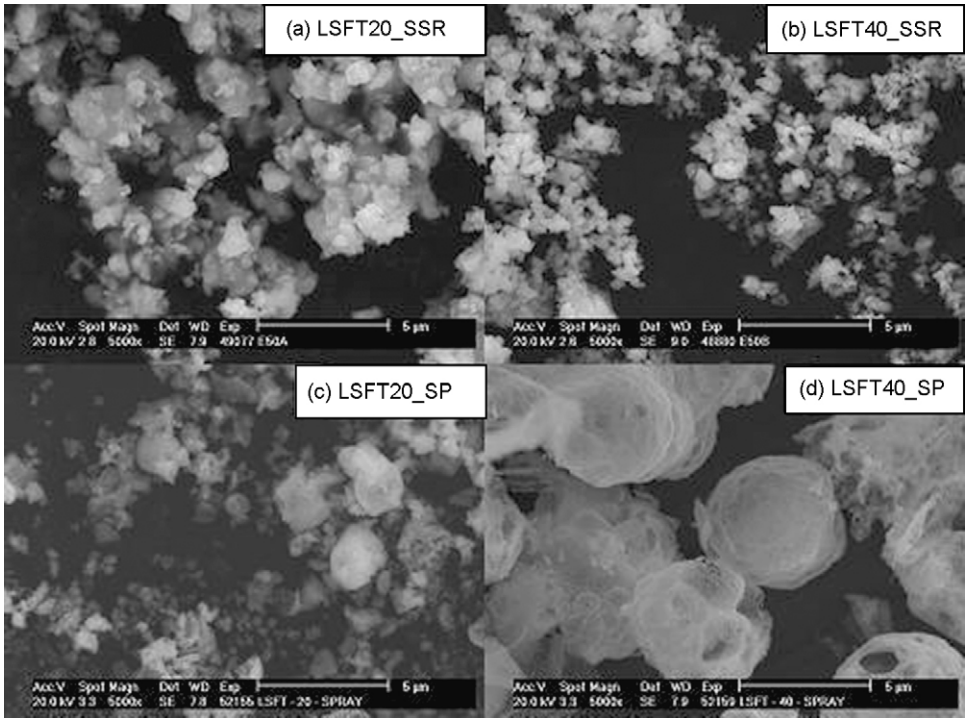

Fig. 2. (a)–(d) SEM micrographs of milled and calcined LSFT prepared by different method.

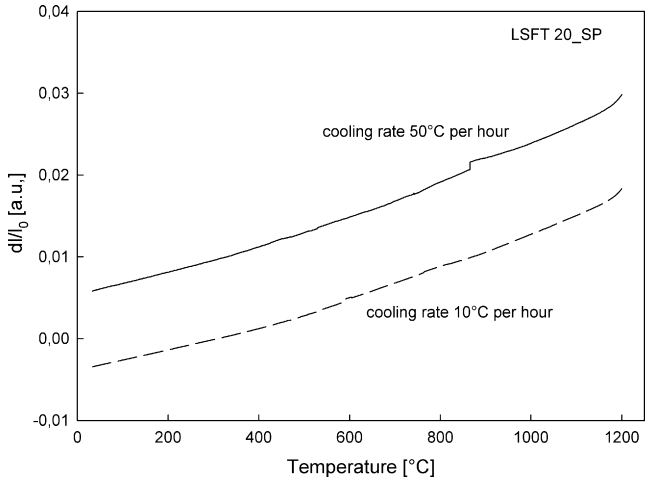

Fig. 4. Dimensional changes of LSFT20_SP sample as measured by dilatometry on cooling. The different cooling rates are given in the figure.

and 220 nm, respectively, Table 1). Samples based on powders prepared by solid state reaction (SSR) give moderately lower density, due to the larger primary particle size (Table 1). The lowest final densities were obtained for LSFT20_SSR powder, consistent with the large particle size (1.09 μm). The dimensional changes of the sintered samples on cooling were measured by dilatometry, the results are given in Fig. 4 for LSFT20-SP cooled at two different cooling rates. Discrete steps in the dilatation curves are due to crack formation caused by tensile stresses building up during cooling (chemical expansion). It can be seen that slower cooling rate means less cracking, probably due to sample being closer to equilibrium and thus lower oxygen concentration gradient across sample. The cooling rates successfully used in this work to obtain crack free sintered bodies ranged from 9 to 15 °C/h.

The dilatometric curves of sintered LSFT 20_SP and LSFT40_SP samples are given in Fig. 5. Based on data in Fig. 5 thermal expansion coefficients were calculated for both compositions and the values are given in Table 3. Below 300 °C both compositions have similar TEC ($13.5 \times 10^{-6}\,K^{-1}$).

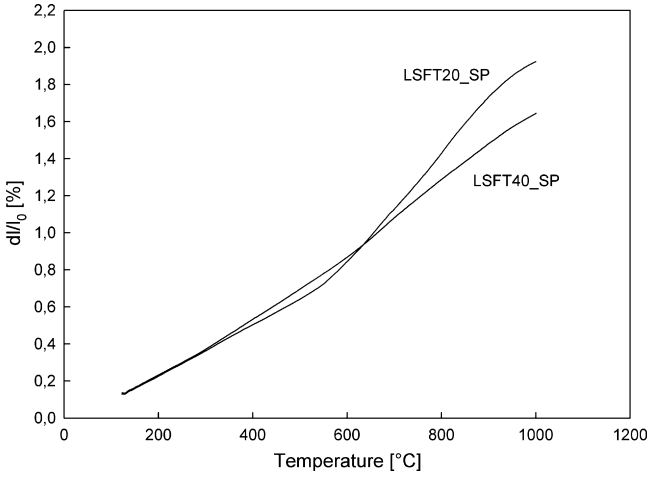

Fig. 5. Dilatometry curves for sintered samples of LSFT20_SP and LSFT40_SP. Data are obtained on heating and applied cooling rate is 5 °C/h.

Table 3
Calculated TEC values in different temperature regions.

Temperature range (°C)	LSFT20_SP ($\times 10^{-6}\,K^{-1}$)	LSFT40_SP ($\times 10^{-6}\,K^{-1}$)
100–300	13.52	13.53
300–600	13.79	16.45
600–800	28.86	21.34

The effect of Ti-substitution was evident at higher temperatures: while LSFT40 showed a gradual and continuous increase in TEC, LSFT20 showed an almost temperature independent TEC below 600 °C with a significant increase above 600 °C ($28.9 \times 10^{-6}\,K^{-1}$ between 600 and 800 °C). The lower TEC value for LSFT40 at temperatures between 600 and 800 °C can be attributed to a lower population of oxygen vacancies due to the higher content of Ti^{4+} at B-site in the perovskite lattice (also cf. Eq. (2) and the discussion in the next section). This behaviour is in accordance with published data for similar compositions such as $La_{0.3}Sr_{0.7}Fe_{0.8}Ti_{0.2}O_{3-\delta}$[14] and $La_{0.5}Sr_{0.5}Fe_{0.9}Ti_{0.1}O_{3-\delta}$.[17]

3.3. Electrical conductivity and oxygen transport properties

The electrical conductivity relaxation measurements were performed in the temperature range from 900 to 1000 °C and at p_{O_2}'s between 0.02 and 0.2 atm. The influence of Ti doping and temperature on total electrical conductivity is given in Fig. 6. LSFT is a p-conductor at high p_{O_2}'s and electronic conductivity is seen to increase with p_{O_2} consistent with the following defect equilibrium:

$$\frac{1}{2}O_2 + V_O^{\cdot\cdot} = O_O^x + 2h \quad (1)$$

It is also seen from Fig. 6 that the conductivity for both compositions decrease with increasing temperature, again consistent with Eq. (1) and the shift in equilibrium to the left with formation of oxygen vacancies on the expense of electron holes (h) as temperature increase. Furthermore, it is evident that Ti has a pronounced effect on the conductivity giving a significant increase as Ti-substitution change from 40% to 20%. Assuming

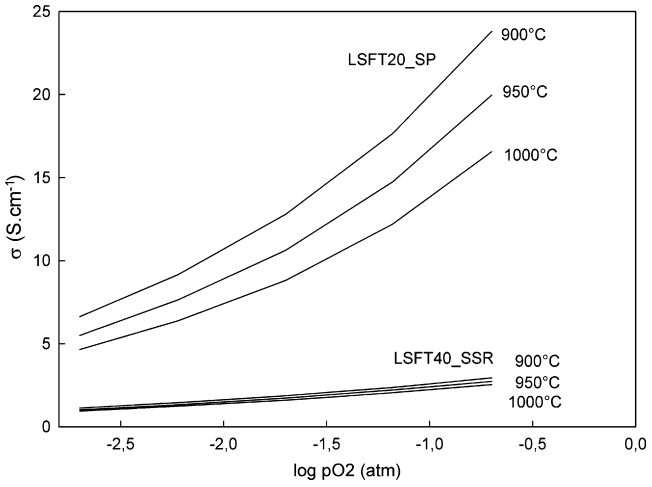

Fig. 6. The electrical conductivity change with p_{O_2}, temperature and % Ti.

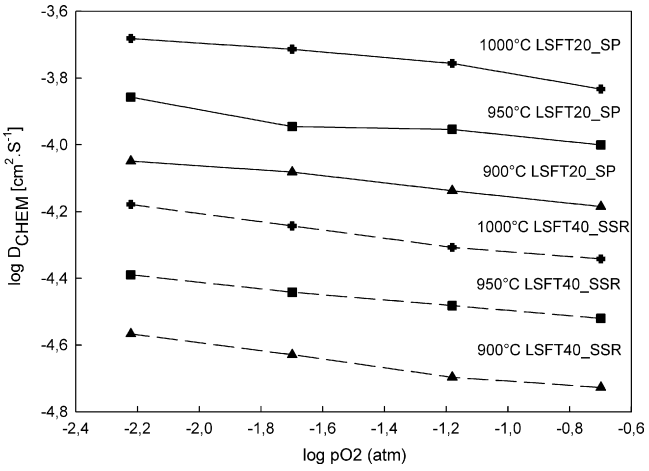

Fig. 7. D_{chem} for a reduction process in terms of oxygen partial pressure (p_{O_2}) for LSFT20 ($La_{0.2}Sr_{0.8}Fe_{0.8}Ti_{0.2}O_{3-\delta}$ – SP) and LSFT40 ($La_{0.2}Sr_{0.8}Fe_{0.6}Ti_{0.4}O_{3-\delta}$ – SSR).

that 3-valent Fe on B-site is substituted by 4-valent Ti the charge balance may be formulated viz.[5]

$$[Sr'_{La}] = 2[V_O^{\cdot\cdot}] + [Ti_{Fe}^{\cdot}] + h \quad (2)$$

That is, in principle the increase in Ti will be on the expense of either electron holes ($h = Ti_{Fe}^{\cdot}$) or oxygen vacancies or both. Fig. 6 does suggest that at the given temperatures and oxygen partial pressures Ti will lower the amount of p-charge carriers. The reported conductivities are all in accordance with conductivities reported elsewhere for similar compositions.[5,14–18]

The bulk diffusion properties (D_{chem}) for both compositions are summarised in Figs. 7 and 8. There are no obvious differences between diffusion coefficients determined by a reduction (Fig. 7) or an oxidation (Fig. 8) relaxation step; they are all within the uncertainty of the method. Generally the bulk diffusion coefficients are seen to decrease with increasing p_{O_2} and % Ti substitution while increasing with temperature. The following relation is valid between bulk diffusion, D_{chem}, and oxygen self-diffusion, D_O[21]

$$D_{chem} = D_O W_O \quad (3)$$

where W_O is the so-called thermodynamic factor[21]:

$$W_O = \frac{1}{2}\left(\frac{\partial \ln p_{O_2}}{\partial \ln c_O}\right) \quad (4)$$

where c_O is the concentration of oxygen in the bulk phase. Furthermore, the following relationship is valid between the self-diffusion coefficients for oxygen (D_O) and oxygen vacancies ($D_{V_O^{\cdot\cdot}}$), respectively[22]:

$$D_O = D_{V_O^{\cdot\cdot}}[V_O^{\cdot\cdot}] \quad (5)$$

At moderate concentration of oxygen vacancies (no interaction between them) $D_{V_O^{\cdot\cdot}}$ is independent of $[V_O^{\cdot\cdot}]$ corresponding to D_O being proportional with $[V_O^{\cdot\cdot}]$.[22] Combining Eqs. (3) and (5) the bulk diffusion coefficient, D_{chem}, may be expressed as

$$D_{chem} = D_{V_O^{\cdot\cdot}}[V_O^{\cdot\cdot}]W_O \quad (6)$$

If the variation in oxygen stoichiometry with partial pressure oxygen is established, the thermodynamic factor, W_O, may be assessed via Eq. (4). Specific oxygen stoichiometry data is not available for the compositions in questions; however, Park and Jacobson[18] have reported data for similar compound (45% Ti) and the assumption of a constant W_O in the narrow p_{O_2}-range reported in Figs. 7–10 is justified. The p_{O_2} independency of both the thermodynamic factor (W_O) and the oxygen vacancy self diffusion coefficient ($D_{V_O^{\cdot\cdot}}$) converts Eq. (6) to the following simple relation between bulk diffusion and population of oxygen vacancies:

$$D_{chem} = \propto [V_O^{\cdot\cdot}] \quad (7)$$

Figs. 7 and 8 clearly show that D_{chem} do increase with decreasing p_{O_2} consistent with Eq. (7) and the increasing population of oxygen vacancies. Since there is a significant decrease in D_{chem} as the amount of Ti in LSFT increase, substitution of Ti on B-site obviously also "consume" oxygen vacancies in accordance with Eq. (2). This is also confirmed by Kaus et al.[5]

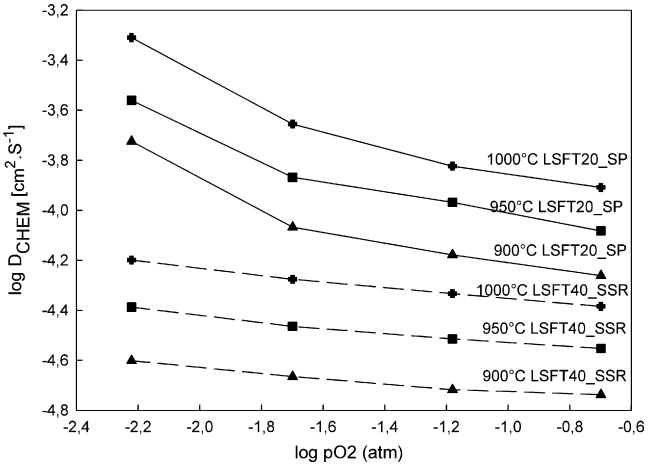

Fig. 8. D_{chem} for an oxidation process in terms of oxygen partial pressure (p_{O_2}) for LSFT20 ($La_{0.2}Sr_{0.8}Fe_{0.8}Ti_{0.2}O_{3-\delta}$ – SP) and LSFT40 ($La_{0.2}Sr_{0.8}Fe_{0.6}Ti_{0.4}O_{3-\delta}$ – SSR).

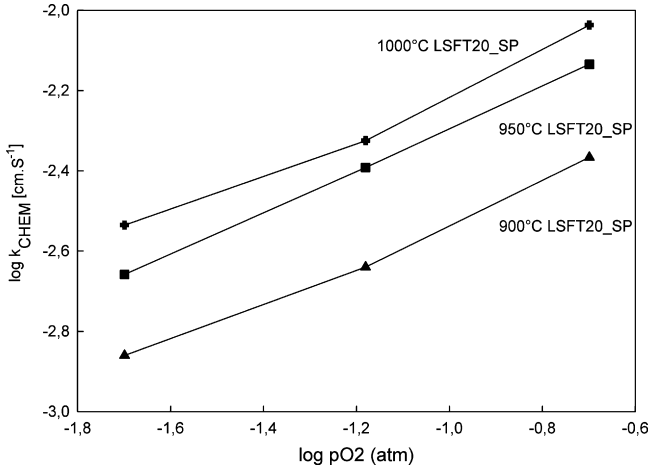

Fig. 9. k_{chem} for a reduction process in terms of oxygen partial pressure (p_{O_2}) for LSFT20 ($La_{0.2}Sr_{0.8}Fe_{0.8}Ti_{0.2}O_{3-\delta}$ – SP).

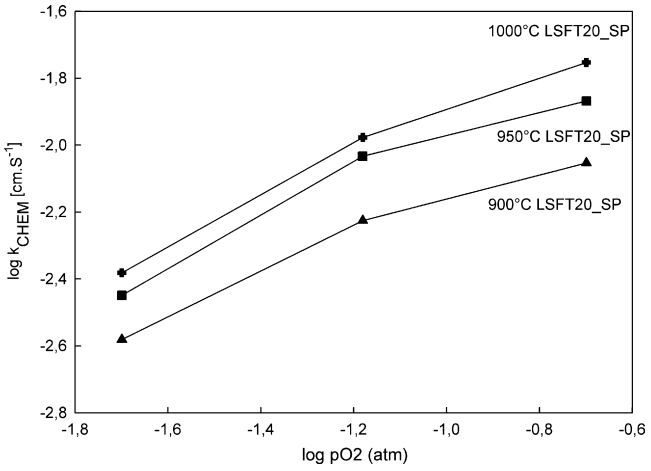

Fig. 10. k_{chem} for an oxidation process in terms of oxygen partial pressure (p_{O_2}) for LSFT20 ($La_{0.2}Sr_{0.8}Fe_{0.8}Ti_{0.2}O_{3-\delta}$ – SP).

Oxygen surface exchange coefficients (k_{chem}) for the composition with 20% Ti are summarised in Figs. 9 and 10, surface exchange data for compositions with 40% is in preparation and will be published elsewhere [in preparation]. Evidently, surface exchange coefficients extracted from reduction steps (Fig. 9) is less than coefficients resulting from oxidation steps (Fig. 10), which reflect the different reaction mechanisms and kinetics involved with oxidation and reduction processes, respectively. Another characteristic feature is the increase in k_{chem} with p_{O_2}, which is in accordance with observations reported for a large number of related oxides[11]. The magnitude of k_{chem} values reported here are also comparable to values reported for similar compounds elsewhere.[11]

The consequence of the bulk diffusion and surface exchange properties reported in this work may be signified by estimating the characteristic thickness, L_C:

$$L_C = \frac{D_O}{k_O} \tag{8}$$

Eq. (8) is derived and discussed by Bouwmeester et al.[23] k_O is similar to the tracer diffusion coefficient, often denoted k^*, and is related to k_{chem} via W_O in the same way as D_{chem} (Eq. (3)), that is

$$L_C = \frac{D_{chem}}{k_{chem}} \tag{9}$$

Using data reported in, e.g., Figs. 7 and 9 (reduction) for mild reducing conditions (p_{O_2} ca. 0.02 atm) at 1000 °C the estimated characteristic thickness is approx. 630 μm. L_C will however increase at even lower oxygen partial pressures and decrease at even higher p_{O_2}'s. That is, e.g., for oxygen permeation membrane applications the estimation of critical thickness gives some useful guidelines concerning the thickness beyond which the flux is controlled only by surface exchange.

4. Conclusion

Phase pure perovskites $La_{0.2}Sr_{0.8}Fe_{1-x}Ti_xO_{3-\delta}$ ($x = 0.2, 0.4$) were synthesized by spray pyrolysis and solid state synthesis followed by calcinations and milling. All synthesized powders were suitable for further dry pressing and pressureless sintering of dense (>96% t.d.) bodies. Powders prepared by spray pyrolysis had smaller particle size (140–220 nm) resulting in final density close to 99% t.d.

To avoid cracking due to chemical expansion it was found that very slow cooling rate (ca 15 °C/h) was necessary at temperatures below 800 °C. The thermal expansion coefficient between 600 and 800 °C was strongly dependent on the substitution level of Ti (21×10^{-6} K^{-1} for 40% Ti^{4+} on B-site and 29×10^{-6} K^{-1} for 20% Ti^{4+} on B-site).

The total electrical conductivity was found to decrease with increasing temperature and substitution level of Ti, while an increase was observed with increasing partial pressure of oxygen. The bulk diffusion coefficient (D_{chem}) decreased with p_{O_2} and substitution level of Ti. This behaviour was explained by a simple defect model, showing that bulk diffusion was basically governed by oxygen vacancies. The combination of surface exchange data and bulk diffusion suggested that the characteristic thickness, L_C, for $La_{0.2}Sr_{0.8}Fe_{0.8}Ti_{0.2}O_{3-\delta}$ at 1000 °C and mild reducing conditions was 630 nm.

Study of transport behaviour in the LSFT system is in progress.

Acknowledgements

This work was supported by the Czech Ministry of Education under grants OC102 (COST 539 Action) and MSM 0021630508.

The authors gratefully acknowledge the funding provided by EEA Financial Mechanism and Norwegian Financial Mechanism.

References

1. Chick, L. A., Maupin, G. D. and Pederson, R. L., Glycine-nitrate synthesis of a ceramic–metal composite. *Nanostruct. Mater.*, 1994, **4**(5), 603–615.
2. Xu, Q., Huang, D., Chen, W., Zhang, F. and Wang, B., Structure, electrical conducting and thermal expansion properties of $Ln_{0.6}Sr_{0.4}Co_{0.2}Fe_{0.8}O_3$ (Ln = La, Pr, Nd, Sm) perovskite-type complex oxides. *J. Alloys Compd.*, 2007, **429**(1–2), 34–39.
3. Zhu, G., Fang, X., Xia, Ch. and Liu, X., Preparation and electrical properties of $La_{0.4}Sr_{0.6}Ni_{0.2}Fe_{0.8}O_3$ using a glycine nitrate process. *Ceram. Int.*, 2007, **31**(1), 115–119.
4. Park, C. Y. and Jacobson, A. J., Thermal and chemical expansion properties of $La_{0.2}Sr_{0.8}Fe_{0.55}Ti_{0.45}O_{3-x}$. *Solid State Ionics*, 2005, **176**(35–36), 2671–2676.
5. Kaus, I., Wiik, K., Kleveland, K., Krogh, B. and Aasland, S., Oxygen transport properties in $La_{1-x}Sr_xFe_{1-y}M_yO_{3-\delta}$ (M = Cr, Ti), $0.2 < x < 0.8$, $0.2 < y$Ti < 0.5, $0.1 < y$Cr < 0.3. *Solid State Ionics*, 2007, **178**(11–12), 817–826.
6. Song, Y. W., Ma, Y., Xiong, H., Jia, Y. Q., Liu, M. L., Jin, M. Z. *et al.*, Synthesis, crystal structure, Mossbauer spectra and dielectric property of $La_{1-x}Sr_xFe_{1-x}Ti_xO_3$ ($x = 0, 0.1, 0.3, 0.5, 0.7, 1$). *Mater. Chem. Phys.*, 2003, **78**(3), 660–665.
7. Patil, P. S., Versatility of chemical spray pyrolysis technique. *Mater. Chem. Phys.*, 1999, **59**(3), 185–198.
8. Mokkelbost, T., Andersen, Ø., Strøm, R. A., Wiik, K., Grande, T. and Einarsrud, M.-A., High-temperature proton-conducting $LaNbO_4$-based materials: powder synthesis by spray pyrolysis. *J. Am. Ceram. Soc.*, 2007, **90**(11), 3395–3400.

9. Norby, T., Haugsrud, R., Marion, S., Einarsrud, M.-A., Wiik, K., Andersen, Ø. *et al.*, *Proton Conductors*, Pub. No.: WO/2006/066918, International Application No.: PCT/EP2005/01387.
10. Rothschild, A., Menesklou, W., Tuller, H. L. and Ivers-Tiffe', E., Electronic structure, defect chemistry, and transport properties of $SrTi_{1-x}Fe_xO_{3-y}$ solid solutions. *Chem. Mater.*, 2006, **18**(16), 3651–3659.
11. Yoo, J., Verma, A., Wang, S. and Jacobson Allan, J., Oxygen transport kinetics in $SrFeO_{3-\delta}$, $La_{0.5}Sr_{0.5}FeO_{3-\delta}$, and $La_{0.2}Sr_{0.8}Cr_{0.2}Fe_{0.8}O_{3-\delta}$ measured by electrical conductivity relaxation. *J. Electrochem. Soc.*, 2005, **152**(3), A497–A505.
12. Wang, S., van der Heide, P. A. W., Chavez, C., Jacobson, A. J. and Adler, S. B., An electrical conductivity relaxation study of $La_{0.6}Sr_{0.4}Fe_{0.8}CO_{0.2}O_{3-\delta}$. *Solid State Ionics*, 2003, **156**(1–2), 201–208.
13. Bayraktar, D., Clemens, F., Diethelm, S., Graule, T., Van herle, J. and Holtappels, P., Production and properties of substituted $LaFeO_3$-perovskite tubular membranes for partial oxidation of methane to syn-gas. *J. Eur. Ceram. Soc.*, 2007, **27**(6), 2455–2461.
14. Fagg, D. P., Kharton, V. V., Frade, J. R. and Ferreira, A. A. L., Stability and mixed ionic-electronic conductivity of (Sr, La)(Ti, Fe)$O_{3-\delta}$ perovskites. *Solid State Ionics*, 2003, **156**(1–2), 45–57.
15. Fagg, D. P., Waerenborgh, J. C., Kharton, V. V. and Frade, J. R., Redox behavior and transport properties of $La_{0.5-x}Sr_{0.5-x}Fe_{0.4}Ti_{0.6}O_{3-\delta}$ ($0 < x < 0.1$) validated by Mossbauer spectroscopy. *Solid State Ionics*, 2002, **146**(1–2), 87–93.
16. Fagg, D. P., Kharton, V. V., Kovalevsky, A. V., Viskup, A. P., Naumovich, E. N. and Frade, J. R., The stability and mixed conductivity in La and Fe doped $SrTiO_3$ in the search for potential SOFC anode materials. *J. Eur. Ceram. Soc.*, 2001, **21**(10–11), 1831–1835.
17. Tsipis, E. V., Patrakeev, M. V., Kharton, V. V., Yaremchenko, A. A., Mather, G. C., Shaula, A. L. *et al.*, Transport properties and thermal expansion of Ti-substituted $La_{1-x}Sr_xFeO_{3-\delta}$ ($x = 0.5$–0.7). *Solid State Sci.*, 2005, **7**(4), 355–365.
18. Park, C. Y. and Jacobson, A. J., Electrical conductivity and oxygen nonstoichiometry of $La_{0.2}Sr_{0.8}Fe_{0.55}Ti_{0.45}O_{3-\delta}$. *J. Electrochem. Soc.*, 2005, **152**(7), J65–J73.
19. Hayashi, H., Suzuki, M. and Inaba, H., Thermal expansion of Sr- and Mg-doped $LaGaO_3$. *Solid State Ionics*, 2000, **128**, 131–139.
20. Trunec, M. and Maca, K., Compaction and pressureless sintering of zirconia nanoparticles. *J. Am. Ceram. Soc.*, 2007, **90**(9), 2735–2740.
21. Weppner, W. and Huggins, R. A., Determination of the kinetic parameters of mixed-conducting electrodes and application to the system Li_3Sb, *J. Electrochem. Soc.*, 1977, **24**, 1569.
22. Kofstad, P., *Nonstoichiometry, Diffusion and Electrical Conductivity of Binary Metal Oxides*. John Wiley & Sons Inc., 1972, 0-471-49776-2.
23. Bouwmeester, H. J. M., Kruidhof, H. and Burgraaf, A. J., Importance of the surface exchange kinetics as rate limiting step in oxygen permeation through mixed-conducting oxides. *Solid State Ionics*, 1994, **72**, 185.